Journal of the Ceramic Society of Japan 122 [5] 361-366 2014 Technical report

Electrospray deposition and characterization of Cu_2O thin films with ring-shaped 2-D network structure

Hiroyuki ITOH, Yoshikazu SUZUKI,[*,†] Tohru SEKINO,[**] Jean-Christophe VALMALETTE[***] and Susumu TOHNO[‡]

Graduate School of Energy Science, Kyoto University, Yoshida Honmachi, Sakyo-ku, Kyoto 606–8501, Japan
[*]Faculty of Pure and Applied Sciences, University of Tsukuba, Tsukuba, Ibaraki 305–8573, Japan
[**]Institute of Multidisciplinary Research for Advanced Materials (IMRAM), Tohoku University, 2–1–1 Katahira, Aoba-ku, Sendai 980–8577, Japan
[***]Université de Toulon / CNRS, IM2NP (UMR 7334), BP 20132, F-83957 La Garde, France

Cu_2O is a p-type semiconductor with a direct band gap of ~2.1 eV, and is expected for solar cell applications etc. Since monovalent Cu is necessary, compositional control is a key step for Cu_2O processing. Electrospray is a phenomenon generating ultrafine droplets, when a high voltage is applied to the surface of liquid. In this study, Cu_2O thin films with unique ring-shaped 2-D network structure have been prepared by using electrospray pyrolysis method. Copper (II) acetate monohydrate, $(CH_3COO)_2Cu{\cdot}H_2O$ was used as a raw material, and D(+) glucose was used as a reducing agent for the reaction from Cu^{2+} to Cu^{+}. At the substrate temperature of 300°C, only Cu_2O was obtained as a crystalline phase. Microstructure, sheet resistance and some optical properties will be discussed.

Key-words : Cu_2O, Cuprous oxide, Electrospray, Pyrolysis

[Received January 10, 2014; Accepted March 13, 2014]

1. Introduction

Cu_2O, cuprous oxide, is a low-cost p-type semiconductor with a direct band gap of ~2.1 eV. Cu_2O is generally less toxic than semiconductors containing Cd or Se, and is expected for solar cell applications etc. Minami et al.[1] recently reported that they successfully fabricated a ZnO/Cu_2O heterojunction solar cell with a conversion efficiency of 3.83%. Furthermore, Darvish and Atwater[2] reported that theoretical efficiencies of Cu_2O/Si and $Cu_2O/GaAs$ dual junction solar cells are calculated to be 27.11 and 30.08%, respectively. Since Cu_2O has relatively high carrier mobility of $>100\,cm^2/Vs$ among p-type semiconductors,[3] a thin-film transistor application is also expected.[4] To produce Cu_2O thin films, various methods have been used, such as radio-frequency magnetron sputtering,[5] thermal oxidation of copper films,[6] molecular beam epitaxy,[7] and electrodeposition.[8] Although these methods have their own advantages, they usually require complex operation, high vacuum or high temperatures, resulting in high-cost and/or low throughput processing. Since monovalent Cu is necessary, compositional control, i.e., oxidation or reduction, is a key step for Cu_2O processing. In addition, rapid processing is desired for actual applications such as solar cell's active layer and thin-film transistor. Kosugi and Kaneko[9] reported spray-pyrolysis deposition of homogeneous Cu_2O thin films (composed of ~50 nm grains) on glass substrates using copper (II) acetate, glucose, and 2-propanol. They succeeded in preparing p-type Cu_2O with the resistivity of $\sim 100\,\Omega cm$.

Electrospray is a phenomenon generating ultrafine droplets, when a high voltage is applied to the surface of liquid.[10),11] When the voltage of several kV is applied between a liquid-supplying capillary and a counter electrode, semispherical liquid at the tip of capillary nozzle receives electrostatic force as well as surface tension and gravity. The resultant force distorts the liquid into a cone shape, and then, a spray of ultrafine droplets is generated. With controlling the quantity of electricity depending on the liquid supply, continuous and uniform droplets can be obtained. An advantage of this method is that the size of the droplets ranges from nm to mm order, depending on the liquid flow rate, electric conductivity of the liquid and applied voltage. Electrospray has attracted much attention in nanotechnology fields, such as nanoparticle evaluation[12] and nanoparticle transport.[13] Furthermore, electrospray pyrolysis, a combined process of electrospray and in situ heat treatment, is currently used for the synthesis of nanoparticles[14)–16] and porous thin films e.g. for lithium ion batteries,[17] fuel cell electrodes,[18] PZT actuators,[19] CdS-based solar cells,[20] and gas sensors.[21] It is expected that the electrospray pyrolysis method can be applicable to form Cu_2O thin film. Up to now, the electrospray pyrolysis method has not yet been applied to Cu_2O thin film processing to the best of our knowledge. In this study, Cu_2O thin films with unique ring-shaped 2-D network structure have been prepared by using electrospray pyrolysis method. The microstructure, electrical property and optical property of the thin films were evaluated.

2. Experimental procedure

2.1 Precursor solution for Cu_2O thin film

Copper (II) acetate monohydrate, $(CH_3COO)_2Cu{\cdot}H_2O$ (99%, Wako Pure Chemical Industries, Ltd., Osaka, Japan) was used as a raw material, and D(+) glucose (Wako Pure Chemical Industries) was used as a reducing agent for the reaction from Cu^{2+} to

† Corresponding author: Y. Suzuki; E-mail: suzuki@ims.tsukuba.ac.jp
‡ Corresponding author: S. Tohno; E-mail: tohno@energy.kyoto-u.ac.jp

DOI http://dx.doi.org/10.2109/jcersj2.122.361

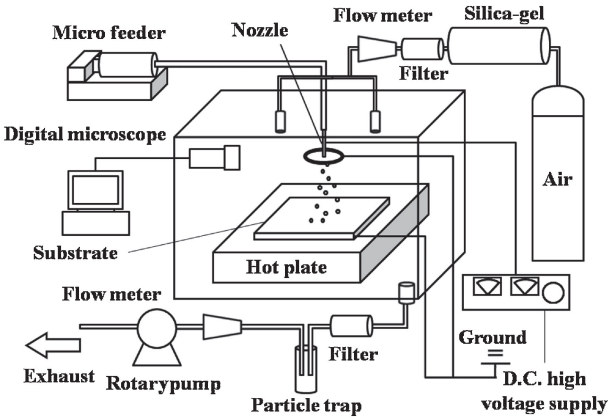

Fig. 1. Schematic illustration of experimental apparatus.

Table 1. Sample numbers and experimental conditions

No.	Cu concentration [mol/L]	Liquid flow rate [mL/h]	Deposition time [min]
1	0.01	2	60
2	0.02	2	30
3	0.04	2	15
4	0.01	1	120
5	0.01	4	30

Cu^+, similarly to the reported work.[9] 0.01–0.04 mol/L copper (II) acetate monohydrate and 0.01 mol/L D(+) glucose were dissolved in 20 vol.% ethanol aqueous solution.

2.2 Electrospray film coating

Figure 1 shows a schematic diagram of the experimental apparatus. It is mainly composed of a syringe pump (Model 100, KD Scientific Inc., MA), an electrospray unit using DC voltage (HSX-10R 1.5, Matsusada Precision Inc., Shiga, Japan), and a hot plate (CHP-170DN, AS ONE Co., Osaka, Japan). The electrospray nozzle (Stainless steel, inner diameter: 0.72 mm, outer diameter: 1.08 mm, SNA-30G-LA, Musashi Engineering Inc., Tokyo, Japan) and the hot plate were set in an acrylic resin chamber with a dry and dust-free air flow (20 L/min). In this study, the voltage was set as 4–5 kV to maintain the stable cone-jet.[20] The droplets are heated and then pyrolyzed on or above a borosilicate glass substrate (Matsunami Glass Ind. Ltd., 12 mm in diameter, 0.12–0.17 mm in thickness, cover glass grade for microscopy based on JIS R 3702, where alkali elution according to JIS R 3502 is <0.2 mg $Na_2O/2.5$ g.). The distance between nozzle tip and substrate was 70 mm. The substrate temperature was changed between 220 and 340°C at the fixed Cu ion concentration of 0.01 mol/L and the fixed liquid flow rate of 2 mL/h. Substrate temperatures were nominally defined as the same as the surface temperatures of the hot-plate, because relatively thin glass substrates (0.12–0.17 mm in thickness) were used in this study. Then, at the fixed substrate temperature of 300°C, Cu ion concentration, liquid flow rate and deposition time were changed so that the total deposition amount became constant (**Table 1**).

2.3 Film evaluation

The microstructure of the Cu_2O film was observed by optical microscopy and by scanning electron microscopy (SEM, SU-6600, Hitachi High-technologies Co., Tokyo, Japan). The constituent phases of the thin film were analyzed by powder X-ray diffractometry (RINT-2100 CMJ, Cu-Kα, 40 kV and 30 mA, XRD, Rigaku, Tokyo, Japan) and by Raman spectroscopy (HR800UV, Horiba, Kyoto, Japan). The resistivity at room temperature was measured by the resistivity/Hall measurement system (ResiTest8300, TOYO Co., Tokyo, Japan) by using Van der Pauw 4-point probe method.[22] The transmittance was measured by UV–Vis spectroscopy (UV-1600, Shimadzu Co. Kyoto, Japan).

3. Results and discussion

3.1 Effect of substrate temperature

Figure 2 shows SEM images of thin films prepared at different substrate temperatures with the fixed Cu ion concentration of 0.01 mol/L and the fixed liquid flow rate of 2 mL/h. As can be seen from Fig. 2, the films deposited at (b) 300°C and (c) 340°C were composed of primary nanoparticles with the diameter of ~20–50 nm, whereas, the nanoparticles were not observed in the film deposited at (a) 260°C. It is considered that, due to the relatively slow liquid evaporation rate at 260°C, deposited small droplets coalesced into large ones, and they formed micron-sized Cu_2O-based grains after the evaporation. The film prepared at 340°C was denser than that at 300°C.

At a low magnification, however, some large particles (around several μm) were also observed in the film prepared at 340°C as shown in Fig. 2(c). Since the diameter evaluation for the droplets (i.e. before the deposition on substrate[15]) did not confirm such large particles, formation of these large particle can be attributed to the high substrate temperature; higher heat radiation from hot-plate may evaporate the droplets not on the substrate surface but above the surface. Then, yielded particles above the hot-plate may attach to the nozzle-tip by the updraft convection from the hot plate, which disturbs the normal electrospraying (*viz*., resulting in the large particle formation). These results suggested that the substrate temperature and the distance between nozzle tip and substrate should be optimized to obtain homogeneous films. **Figure 3** demonstrates the particle size distribution of the film deposited at 300°C in Fig. 2. The geometric mean diameter was rather small, 44.3 nm, and the geometric standard deviation was relatively narrow, 1.21, indicating the substantial monodispersion.

Much lower substrate temperatures were also examined. **Figure 4** shows SEM images of the thin films prepared at 170 and 220°C. Other conditions were the same as those for 260–340°C. At 170°C, the film was gel-like without the formation of nanoparticulates, indicating the insufficient evaporation of the liquid. At 220°C, fine but heterogeneous surface indicated the slow evaporation of the liquid.

Figure 5 demonstrates the XRD patterns of the films prepared at 220, 260, 300, and 340°C. At 220 and 260°C, Cu and Cu_2O were found as crystalline phases. At 300°C, only Cu_2O was confirmed as a crystalline phase. At 340°C, the film was composed of Cu_2O and CuO. Thus, in order to obtain a phase pure Cu_2O film, 300°C was the optimum condition in this study. Reduction by glucose was promoted, at 220–300°C, while oxidation by heating yielded CuO at 340°C. When the distance between nozzle tip and substrate was changed from 7 to 5 cm, the formation of Cu_2O and Cu was confirmed even at 300°C (i.e., similarly to 220 and 260°C cases for the 7 cm distance). This was because the increased liquid deposition on the substrate increased the heat of vaporization and decreased the local temperature of the substrate. This experiment strongly suggests that the control of decomposition temperature is important to obtain phase-pure Cu_2O film.

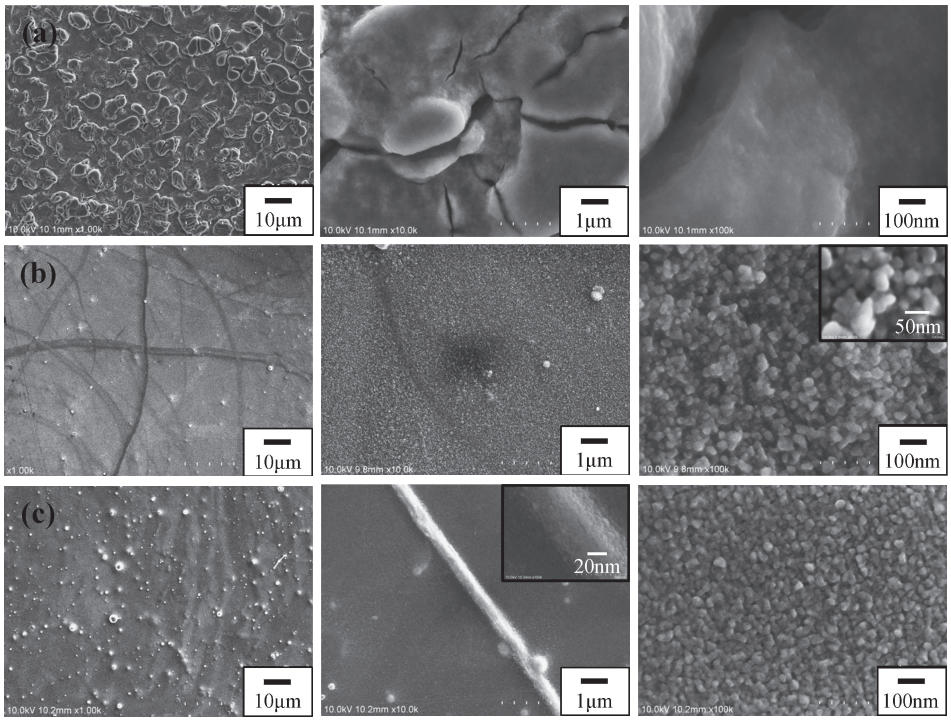

Fig. 2. SEM images of thin films prepared at different temperatures: (a) 260°C, (b) 300°C, and (c) 340°C (left: low magnification, middle: intermediate magnification, right: high magnification).

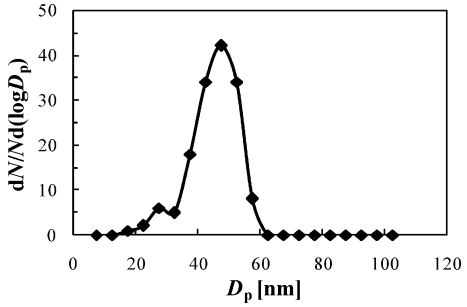

Fig. 3. Particle size distribution of the film prepared at 300°C (solution concentration 0.01 mol/L, liquid flow rate: 2 mL/h). Geometric mean diameter was 44.3 nm, and geometric standard deviation was 1.21.

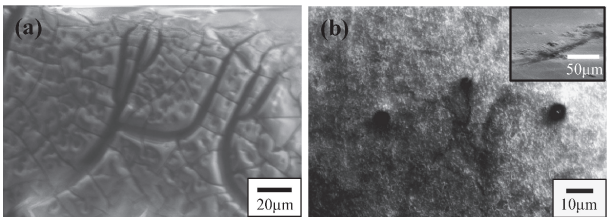

Fig. 4. SEM images of thin films prepared at lower temperatures: (a) 170 and (b) 220°C.

3.2 Effect of solution concentration and liquid flow rate

Then, the effect of the solution concentration and the liquid flow rate were examined. **Figure 6** shows SEM images of thin films prepared at different solution concentrations, 0.01, 0.02 and 0.04 mol/L of metallic (copper) component (Samples 1, 2 and 3 in Table 1). The glucose concentration and the substrate temperature were kept constant as 0.01 mol/L and 300°C, respectively.

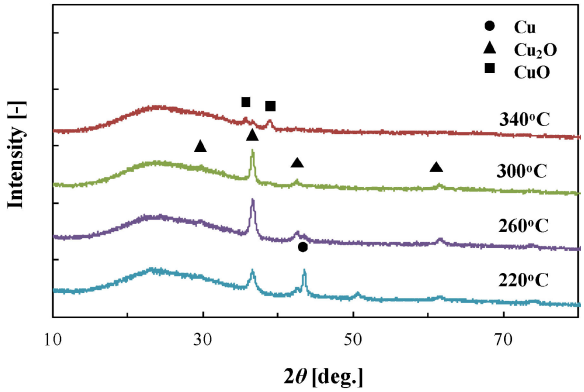

Fig. 5. XRD patterns of thin films prepared at different temperatures.

With increasing the metallic concentration (and concurrently decreasing the deposition time), the film became inhomogeneous. The films of 0.01 and 0.02 mol/L consisted of fine nanoparticles with diameter of 20–50 nm, while the film of 0.04 mol/L consisted of nanoparticles of ~70 nm. The increase of particle size can be explained by the increase of metallic amount in each droplet.

Figure 7 shows SEM images of thin films prepared at different liquid flow rate, 1, 2, and 4 mL/h with the metallic concentration of 0.01 mol/L (Samples 4, 1 and 5 in Table 1). The glucose concentration and the substrate temperature were kept constant as 0.01 mol/L and 300°C, respectively. With increasing the liquid flow rate (and concurrently decreasing the deposition time), the film macroscopically became inhomogeneous. However, the difference was not so prominent as Fig. 6. At the liquid flow rate of 1 mL/h, some flat and dense regions were observed [Fig. 7(a) left and right]. The longer term deposition (120 min in this case) locally enabled the rearrangement of nanoparticles. On the other

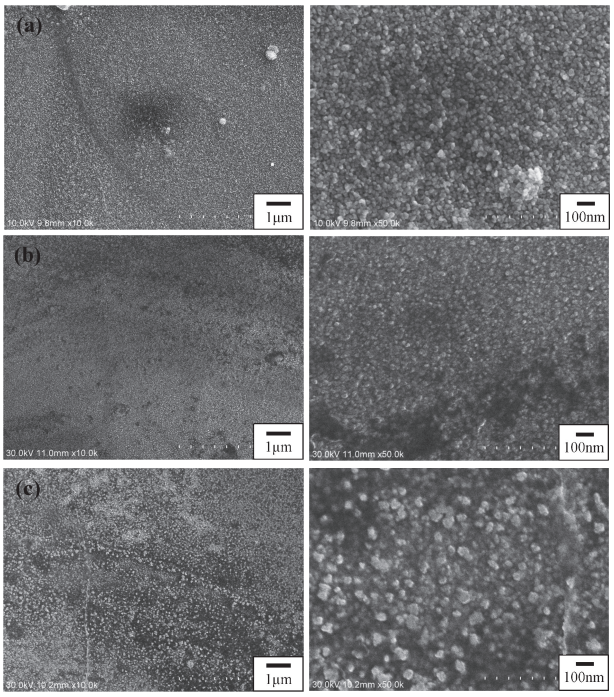

Fig. 6. SEM images of thin films prepared at different solution concentrations: (a) 0.01, (b) 0.02 and (c) 0.04 mol/L of metallic component. The glucose concentration and the substrate temperature were kept constant as 0.01 mol/L and 300°C, respectively.

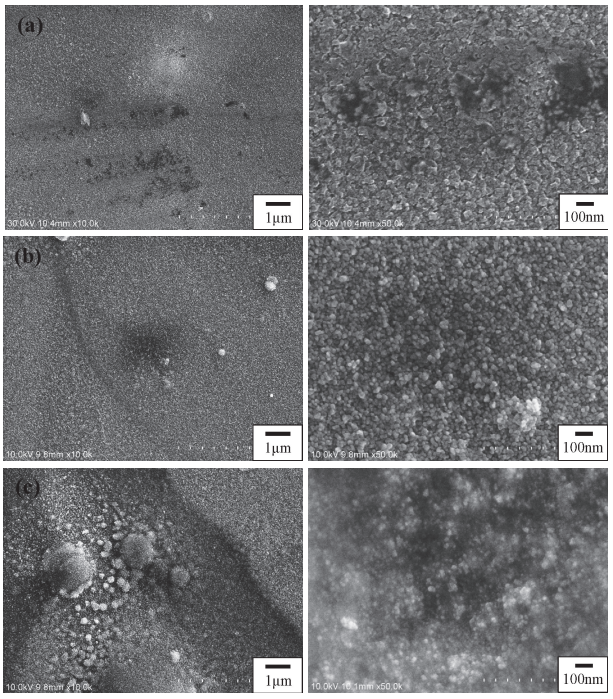

Fig. 7. SEM images of thin films prepared at different liquid flow rates: (a) 1, (b) 2, (c) 4 mL/h. The glucose concentration and the substrate temperature were kept constant as 0.01 mol/L and 300°C, respectively.

hand, at the liquid flow rate of 4 mL/h, the evaporation rate should become slower and some droplets merged with each other. That is why some large particles were found in 4 mL/h sample [Fig. 7(c) left].

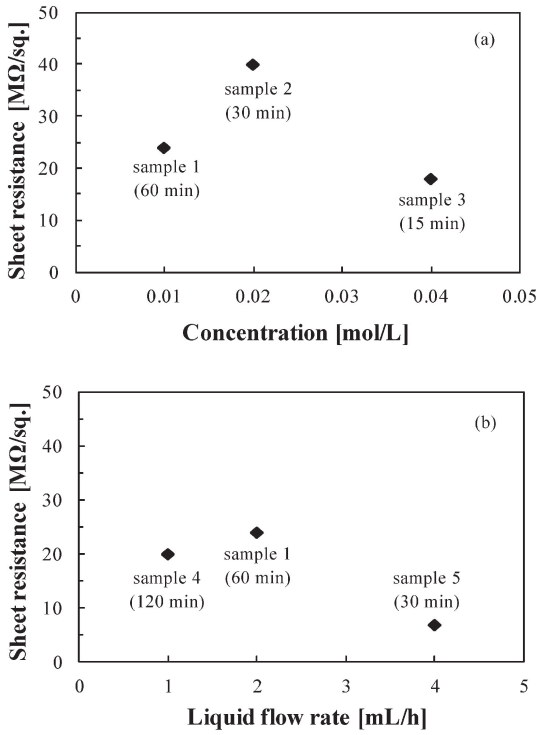

Fig. 8. Sheet resistance of thin films: (a) prepared at different solution concentrations (and different deposition time) with constant liquid flow rate (2 mL/h). (b) prepared at different liquid flow rates (and different deposition time) with constant solution concentration (0.01 M).

3.3 Sheet resistance

Figure 8(a) shows the sheet resistance of films prepared at different solution concentrations (and different deposition time) with constant liquid flow rate (2 mL/h), corresponding to Fig. 6. The lower resistance of 0.01 mol/L than that of 0.02 mol/L can be explained by the denser film formation of 0.01 mol/L as shown in Fig. 6. The lower resistance of 0.04 mol/L might be attributed to the growth of particle size (~70 nm in this case).

Figure 8(b) shows the sheet resistance of films prepared at different liquid flow rates (and different deposition time) with constant solution concentration (0.01 mol/L), corresponding to Fig. 7. Comparing the samples of 1 and 2, the 1 mL/h sample had somewhat lower resistance, probably due to the formation of dense region as shown in Fig. 7(a). The 4 mL/h sample had the lowest resistance. In good agreement with the SEM observation, effect of the liquid flow rate on sheet resistance [Fig. 8(b)] was less prominent than that of the solution concentrations [Fig. 8(a)].

In order to verify the reason of the different sheet resistance, optical microscopic observation was conducted (**Fig. 9**). Although the in-flight droplet size (confirmed by droplet fixation technique[15]) was in the range of several micrometers, Fig. 9 clearly shows the existence of agglomerated large droplets with the diameter of several hundred micrometers. The samples with lower resistance (Samples 3, 4 and 5 in Fig. 8) had thick circular traces after drying, suggesting the formation of networks of conducting paths. The formation of ring-shaped structure is attributable to the drying of coalescent droplets, which is called as "coffee ring effect".[23]

Furthermore, the sample with the highest sheet resistance (Sample 2, 40 MΩ/sq.) and that with the lowest sheet resistance (Sample 5, 6.9 MΩ/sq.) were evaluated by the Raman spectroscopy (**Fig. 10**). For both samples, significant peaks corre-

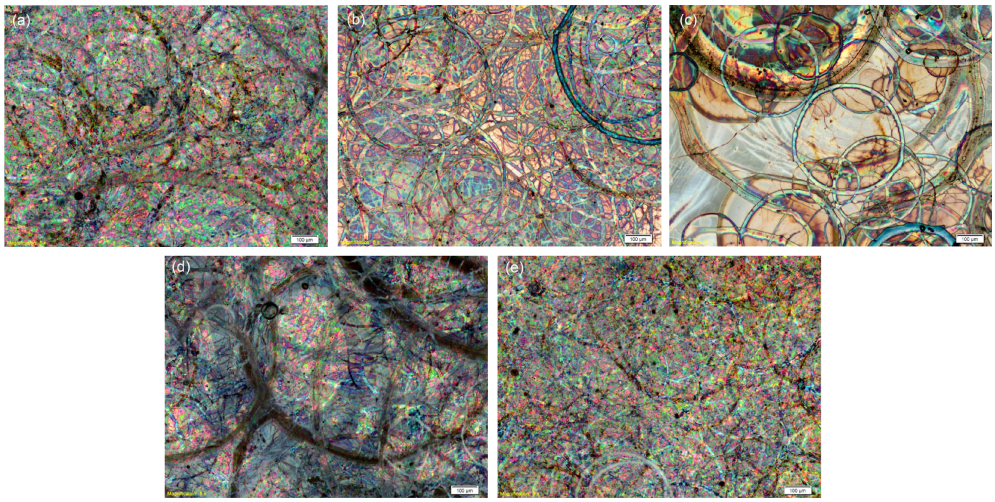

Fig. 9. Optical micrograph of thin films: (a) sample 1 (0.01 mol/L - 2 mL/h - 60 min), (b) sample 2 (0.02 mol/L - 2 mL/h - 30 min), (c) sample 3 (0.04 mol/L - 2 mL/h - 15 min), (d) sample 4 (0.01 mol/L - 1 mL/h - 120 min), (e) sample 5 (0.01 mol/L - 4 mL/h - 30 min).

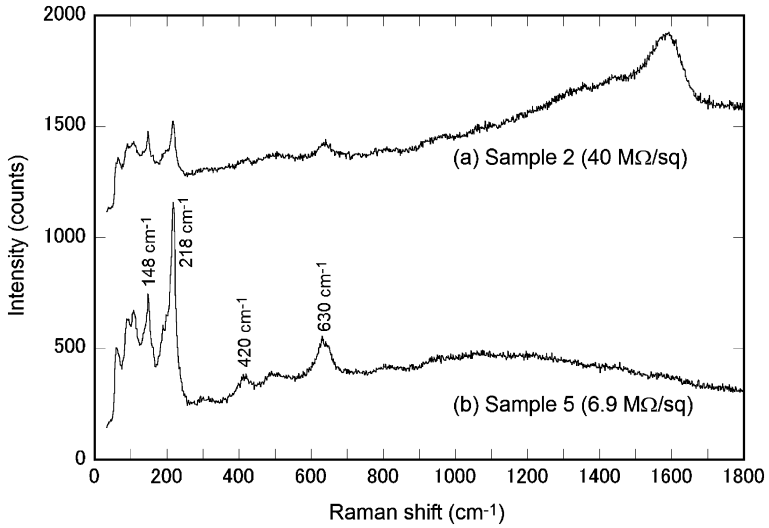

Fig. 10. Raman spectra of selected thin films.

sponding to Cu_2O (148, 218, 420 and 630 cm^{-1}) were observed, but peaks corresponding to CuO (273 and 327 cm^{-1}) were not observed.[24] In the Sample 2, broad peak at 1600 cm^{-1}, corresponding to the residual organic molecules was clearly observed. They are assigned to carbon-containing compounds resulting from incomplete decomposition of precursors during pyrolysis. On the contrary, in the Sample 5, such peak did not exist. The peaks corresponding to Cu_2O (at lower Raman shift) were more prominent for Sample 5. Details of small peaks corresponding to Cu_2O are available in the literature.[25]

3.4 Optical property

All films are yellow and have the absorption in the visible range. **Figure 11**(a) shows the transmittance spectra of films prepared at different solution concentrations (and different deposition time) with constant liquid flow rate (2 mL/h), corresponding to Figs. 6 and 8(a). The film of 0.01 mol/L had 75% transmittance at 830 nm. Higher transmittance of 0.04 mol/L sample (Sample 3) under 600 nm region can be explained by the apparently high "aperture ratio" of this sample as shown in Fig. 9(c).

Figure 11(b) shows the transmittance spectra of films prepared at different liquid flow rates (and different deposition time) with constant solution concentration (0.01 mol/L), corresponding to Figs. 7 and 8(b). The curves of 1 mL/h (Sample 4) and 2 mL/h (Sample 1) were similar to each other, in good agreement with Figs. 7 and 8(b). The slight difference between them can be attributed to the particle packing density (and hence the thickness of the film).

4. Conclusions

In conclusion, in order to prepare a homogeneous and dense Cu_2O thin film by electrospray pyrolysis method, optimum substrate temperature was 300°C. At lower substrate temperature, Cu and Cu_2O were formed, and at higher substrate temperature, CuO and Cu_2O were formed. At 300°C, only Cu_2O was obtained as a crystalline phase. The optimum substrate temperature will be affected by the nozzle tip-substrate distance and the liquid flow rate. When the nozzle tip-substrate distance and the liquid flow rate became larger, the optimum substrate temperature should be somewhat higher.

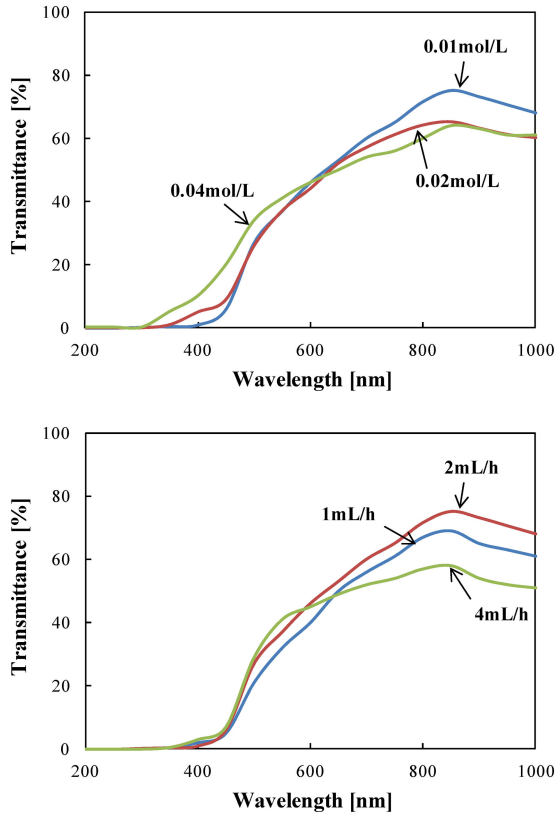

Fig. 11. Transmittance spectra of thin films: (a) prepared at different solution concentrations (and different deposition time) with constant liquid flow rate (2 mL/h). (b) prepared at different liquid flow rates (and different deposition time) with constant solution concentration (0.01 M).

By using electrospray pyrolysis method, particle size and packing density of films can be controlled by changing the solution concentration and liquid flow rate. Dense and homogeneous films exhibited lower resistance (higher conductivity) and lower transmittance. These films can be applicable for semiconductor devices.

Whereas, porous and inhomogeneous films had higher resistance (lower conductivity) and higher transmittance. These films can be applicable for gas sensors, photocatalysts and optical devices. Films with thick circular traces are promising for a p-type transparent conducting oxide.

Sui et al.[26] have recently reported the processing of faceted Cu_2O microcrystals only at <80°C. By combining their crystal growth conditions with our electrospray method, further progress will be expected.

References

1) T. Minami, Y. Nishi, T. Miyata and J. Nomoto, *Appl. Phys. Exp.*, 4, 062301 (2011).
2) D. S. Darvish and H. A. Atwater, Photovoltaic Specialists Conference (PVSC), 2009 34th IEEE, 2195–2199 (2009).
3) B. S. Li, K. Akimoto and A. Shen, *J. Cryst. Growth*, 311, 1102–1105 (2009).
4) E. Fortunato, V. Figueiredo, P. Barquinha, E. Elamurugu, R. Barros, G. Gonçalves, S.-H. K. Park, C.-S. Hwang and R. Martins, *Appl. Phys. Lett.*, 96, 192102 (2010).
5) K. Akimoto, S. Ishizuka, M. Yanagita, Y. Nawa, Goutam K. Paul and T. Sakurai, *Sol. Energy*, 80, 715–722 (2006).
6) A. H. Jayatissa, K. Guo and A. C. Jayasuriya, *Appl. Surf. Sci.*, 255, 9474–9479 (2009).
7) K. Kawaguchi, R. Kita, M. Nishiyama and T. Morishita, *J. Cryst. Growth*, 143, 221–226 (1994).
8) Y. Tang, Z. Chen, Z. Jia, L. Zhang and J. Li, *Mater. Lett.*, 59, 434–438 (2006).
9) T. Kosugi and S. Kaneko, *J. Am. Ceram. Soc.*, 81, 3117–3124 (1998).
10) S. J. Gaskell, *J. Mass Spectroscopy*, 32, 677–688 (1997).
11) I. W. Lenggoro and K. Okuyama, *J. Soc. Powder Technol. Jpn.*, 37, 753–760 (2000).
12) I. W. Lenggoro, B. Xia and K. Okuyama, *Langmuir*, 18, 4584–4591 (2002).
13) N. V. Avseenko, T. Ya. Morozova, F. I. Ataullakhanov and V. N. Morozov, *Anal. Chem.*, 74, 927–933 (2002).
14) A. J. Rulison and R. C. Flagan, *J. Am. Ceram. Soc.*, 77, 3244–3250 (1994).
15) Y. Terada, Y. Suzuki and S. Tohno, *Mater. Res. Bull.*, 47, 889–895 (2012).
16) T. Matsubara, Y. Suzuki and S. Tohno, *C. R. Chim.*, 16, 244–251 (2013).
17) C. H. Chen, E. M. Kelder, M. J. G. Jak and J. Schoonman, *Solid State Ionics*, 86–88, 1301–1306 (1996).
18) I. Taniguchi, R. C. van Landschoot and J. Schoonman, *Solid State Ionics*, 156, 1–13 (2003).
19) J. Lu, J. Chu, W. Huang and Z. Ping, *Sens. Actuators, A*, 108, 2–6 (2003).
20) B. Su and K. L. Choy, *Thin Solid Films*, 359, 160–164 (2000).
21) Y. Matsushima, Y. Nemoto, T. Yamazaki, K. Maeda and T. Suzuki, *Sens. Actuators, B*, 96, 133–138 (2003).
22) L. J. van der Pauw, *Phillips Technical Rev.*, 20, 220–224 (1958).
23) R. D. Deegan, O. Bakajin, T. F. Dupont, G. Huber, S. R. Nagel and T. A. Witten, *Nature*, 389, 827–829 (1997).
24) Y.-K. Hsu, C.-H. Yu, Y.-C. Chen and Y.-G. Lin, *Electrochim. Acta*, 105, 62–68 (2013).
25) H. Solache-Carranco, G. Juárez-Díaz, A. Esparza-García, M. Briseño-García, M. Galván-Arellano, J. Martínez-Juárez, G. Romero-Paredes and R. Peña-Sierra, *J. Lumin.*, 129, 1483–1487 (2009).
26) Y. Sui, W. Fu, H. Yang, Y. Zeng, Y. Zhang, Q. Zhao, Y. Li, X. Zhou, Y. Leng, M. Li and G. Zou, *Cryst. Growth Des.*, 10, 99–108 (2010).